

# Application of the SCC-DFTB Method to Hydroxide Water Clusters and Aqueous Hydroxide Solutions

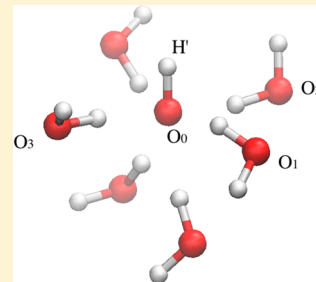
Tae Hoon Choi,<sup>†,||</sup> Ruibin Liang,<sup>§,||</sup> C. Mark Maupin,<sup>‡</sup> and Gregory A. Voth\*,<sup>§</sup>

<sup>†</sup>Department of Chemical Engineering Education, Chungnam National University, Daejeon 305-764, Republic of Korea

<sup>‡</sup>Chemical and Biological Engineering Department, Colorado School of Mines, Golden, Colorado 80401, United States

<sup>§</sup>Department of Chemistry, James Franck Institute, and Computation Institute, University of Chicago, 5735 S. Ellis Ave., Chicago, Illinois 60637, United States

**ABSTRACT:** The self-consistent charge density functional tight binding (SCC-DFTB) method has been applied to hydroxide water clusters and a hydroxide ion in bulk water. To determine the impact of various implementations of SCC-DFTB on the energetics and dynamics of a hydroxide ion in gas phase and condensed phase, the DFTB2, DFTB2- $\gamma^h$ , DFTB2- $\gamma^h$ +gaus, DFTB3-diag, DFTB3-diag+gaus, DFTB3-Full+gaus, and DFTB3-3OB implementations have been tested. Energetic stabilities for small hydroxide clusters,  $\text{OH}^-(\text{H}_2\text{O})_n$ , where  $n = 4-7$ , are inconsistent with the results calculated with the B3LYP and second order Møller–Plesset (MP2) levels of ab initio theory. The condensed phase simulations,  $\text{OH}^-(\text{H}_2\text{O})_{127}$ , using the DFTB2, DFTB2- $\gamma^h$ , DFTB2- $\gamma^h$ +gaus, DFTB3-diag, DFTB3-diag+gaus, DFTB3-Full+gaus and DFTB3-3OB methods are compared to Car–Parrinello molecular dynamics (CPMD) simulations using the BLYP functional. The SCC-DFTB method including a modified O–H repulsive potential and the third order correction (DFTB3-diag/Full+gaus) is shown to poorly reproduce the CPMD computational results, while the DFTB2 and DFTB2- $\gamma^h$  method somewhat more closely describe the structural and dynamical nature of the hydroxide ion in condensed phase. The DFTB3-3OB outperforms the MIO parameter set but is no more accurate than DFTB2. It is also shown that the overcoordinated water molecules lead to an incorrect bulk water density and result in unphysical water void formation. The results presented in this paper point to serious drawbacks for various DFTB extensions and corrections for a hydroxide ion in aqueous environments.



## 1. INTRODUCTION

The energetic and dynamical nature of aqueous systems that contain excess protons and hydroxide (proton hole) has been widely studied due to its fundamental role in acid–base chemistry and biological processes.<sup>1–5</sup> Although the use of high level quantum mechanics (QM) can accurately describe the static potential energy surface of cluster systems and the reactive process of the transfer media in aqueous solution, the high computational cost of QM calculations limits its use in modeling relevant sized systems and/or long time dynamical process.<sup>6</sup> The alternative to full QM calculations is to develop models or employ approximate QM methods such as semiempirical electronic structure methods. These approaches are parametrized using higher level ab initio calculations and their development is still ongoing based on benchmark studies.<sup>7–9</sup>

One of the most widely used approximate QM methods is the self-consistent charge density functional tight binding (SCC-DFTB) method as an approximation to density functional theory (DFT).<sup>9–26</sup> Compared to other semiempirical electronic structure methods such as AM1, PM3, and NDDO,<sup>27–32</sup> the relatively more accurate description of geometries, energies, and vibrational frequencies that SCC-DFTB yields has made it widely utilized for the study of organic, biomolecular systems, and material systems,<sup>23–26</sup> although sometimes without a good degree of accuracy.<sup>33</sup>

Moreover, in our previous simulations based on the released parameter sets at the time for several prototype protonated water clusters including the magic cluster,  $\text{H}^+(\text{H}_2\text{O})_{21}$ , and bulk water in the presence of an excess proton, the SCC-DFTB method gives generally inaccurate results for the protonated clusters, bulk water, and the excess proton in water.<sup>18,19</sup> These studies led to a re-examination by Goyal et al., who suggested that the inaccurate standard  $\gamma_{\text{OH}}$  repulsive potential of the SCC-DFTB method resulted in a reduced proton-transfer barrier, and stabilization of the Zundel form of the hydrated proton over the Eigen form in gas and condensed phase. These authors addressed these shortcomings and some of the properties were marginally improved through the implementation of third order correction and an empirically modified O–H repulsive potential.<sup>20</sup> In the very recent work by Gaus et al., a new parameter set, 3OB, was introduced and showed promising results for benchmark tests in the gas phase.<sup>34</sup> 3OB stands for design for DFTB3 of organic and biological applications while the previous parameter set, MIO, was designed for material and biological system.

In the present work, we evaluate the accuracy of the current SCC-DFTB implementations, including the proposed O–H

Received: January 28, 2013

Revised: April 7, 2013

Published: April 8, 2013



repulsive potential and third order correction with both MIO and the 3OB parameter sets, focusing on both cluster and liquid water systems with the hydroxide ion (proton hole).<sup>35</sup>

For the detailed analysis of the hydroxide cluster, basin hopping Monte Carlo simulations<sup>36–39</sup> are utilized to investigate the low-lying energy minimum structures of the small OH<sup>−</sup> water cluster ion, OH<sup>−</sup>(H<sub>2</sub>O)<sub>n</sub>, for n = 4–7. For the condensed phase, molecular dynamics (MD) simulations of the hydroxide ion in an aqueous environment with Ewald summation long-range electrostatics calculated with the supercell method was utilized.

## 2. COMPUTATIONAL METHODS

**2.1. The SCC-DFTB Method.** The SCC-DFTB method is based on the Taylor expansion of the Kohn–Sham total energy in terms of the charge density fluctuations, with the Hamiltonian matrix elements being evaluated using a minimal basis set of pseudoatomic orbitals, along with a two-center approximation. The energy function for the SCC-DFTB method is expressed as

$$E_{\text{total}}^{\text{SCC-DFTB}} = \sum_{i\mu\nu} c_\mu^i c_\nu^i H_{\mu\nu}^0 + E_{\text{rep}} + \frac{1}{2} \sum_{\alpha\beta} \gamma_{\alpha\beta} \Delta q_\alpha \Delta q_\beta \quad (1)$$

where  $H_{\mu\nu}^0$  are the Hamiltonian matrix elements and  $c_\mu^i$  and  $c_\nu^i$  are the wave function expansion coefficients,  $E_{\text{rep}}$  accounts for short-range repulsive term, and  $\Delta q_\alpha$  and  $\Delta q_\beta$  are the charge fluctuation terms associated with atoms  $\alpha$  and  $\beta$ , respectively. The  $\gamma_{\alpha\beta}$  function is determined by

$$\begin{aligned} \gamma_{\alpha\beta} &= \frac{1}{R_{\alpha\beta}} - S_{\alpha\beta} \times f_{\alpha\beta}, f_{\alpha\beta} \\ &= \begin{cases} \exp\left[-\left(\frac{U_\alpha + U_\beta}{2}\right)^\zeta R_{\alpha\beta}^{-2}\right], & \text{if } (\alpha \text{ or } \beta = \text{H}) \\ \text{or} \\ 1, & \text{else} \end{cases} \quad (2) \end{aligned}$$

where  $S_{\alpha\beta}$  is an exponentially decaying short-range function. The damping function  $f_{\alpha\beta}$  is introduced to correctly describe hydrogen-bonding interactions, where  $U_\alpha$  and  $U_\beta$  are the atomic Hubbard parameters related to the chemical hardness of atoms,  $\alpha$  and  $\beta$ , respectively. The parameter  $\zeta$  is determined by fitting to hydrogen bonding energies for select clusters from high level QM calculations.

The third order correction term was initially introduced with only the on-site third order term, and the complete third-order term has been recently implemented in gas phase calculations.<sup>21</sup> In the present study, we considered two types of third order DFTB corrections, the first being the on-site third order correction and the second being full third order correction. The two corrections are described by

$$E_{\text{on-site}}^{\text{3rd}} = \frac{1}{6} \sum_{\alpha} U_{\alpha}^d \Delta q_{\alpha}^3 \quad (3)$$

$$E_{\text{Full}}^{\text{3rd}} = \frac{1}{3} \sum_{\alpha\beta} \Gamma_{\alpha\beta} \Delta q_{\alpha}^2 \Delta q_{\beta} \quad (4)$$

respectively, where  $U_{\alpha}^d$  is the charge derivative of the atomic Hubbard parameter  $U_{\alpha}$  and  $\Gamma_{\alpha\beta}$  describe derivatives of  $\gamma$  function with respect to atomic charges. The full correction is an extension of the on-site correction and was shown to

improve hydrogen bonding energies and proton affinities over the latter.<sup>21</sup> Furthermore, the O–H repulsive potential has been modified for better description of proton transport (PT) barrier, and represented as follows:

$$U_{\text{OH}}^{\text{Rep}}(R) = U_{\text{OH}}^{\text{Rep, std}}(R) + a_1 \exp\left[-\frac{(R - a_2)^2}{a_3}\right] S(R) \quad (5)$$

where  $S(R)$  is the switching function and the parameters,  $a_1$ ,  $a_2$ , and  $a_3$  were optimized using a genetic algorithm and the SCC-DFTB potential including the hydrogen-bonding correction. A more detailed description can be found in refs 16 and 20.

In ref 34, a new parameter set named 3OB was designed, where both electronic parameters and repulsive potential parameters (appearing in the first and second term in eq 1, respectively) are optimized for full third order SCC-DFTB calculations. In gas phase calculations, it was shown to outperform the old MIO parameter set due to an improved geometry of nonbonded interactions and reduction of the overbinding errors. The effect of replacing MIO with the 3OB parameter set in the third order SCC-DFTB calculations will also be investigated in this work.

In the following sections, we will use the same notations from ref 20 for denoting the different variants of the SCC-DFTB method. The standard second-order SCC-DFTB as expressed in eq 1 will be denoted as “DFTB2”, the hydrogen-bonding correction is indicated by adding “-γ”. The third order DFTB methods with the on-site third order correction (eq 3) and with full third order correction (eq 4) are expressed as “DFTB3-diag” and “DFTB3-Full”, respectively. Those DFTB methods using a modified O–H repulsive potential (eq 5) are indicated by the additional “gaus” keyword. The above notation applies to the SCC-DFTB methods using the MIO parameter set while the third order DFTB method using the new 3OB parameter set will be denoted as “DFTB3-3OB”. All third order methods used in this study include the hydrogen-bonding correction. In the case of the cluster simulations, the dispersion interaction term is added because it plays a major role in determining the low-energy minima based on our benchmark calculations with neutral and protonated water clusters.<sup>18</sup>

**2.2. Cluster Simulation Setup.** The basin-hopping Monte Carlo method uses Monte Carlo walks combined with gradient-based optimizations to locate local potential energy minima. At each move, the structure is optimized to the local minimum in its “basin”, and acceptance of moves is based on the energies of the minima. As a result, barriers are effectively bypassed, making this an efficient approach for searching for low-energy minima. In the present study, the Monte Carlo moves involve both translational and rotational moves at a reduced temperature of 2.0 kJ/mol, with a target acceptance ratio of 0.4, which has been shown to work reasonably well.<sup>18</sup> At each Monte Carlo step, the number of molecules to be moved was chosen at random. Randomly selected initial structures of OH<sup>−</sup>(H<sub>2</sub>O)<sub>n</sub> with n = 4–7, were then selected and subsequently used to carry out eight independent sets of the basin hopping Monte Carlo runs of 100,000 steps each.

**2.3. Molecular Dynamics Setup.** An initial bulk water system was created by simulating 128 modified TIP3P classical water molecules for 500 ps of molecular dynamics (MD) in the constant NVE ensemble followed by 500 ps in the constant NPT ensemble. The NPT pre-equilibration simulations resulted in box dimensions of 15.8 × 15.8 × 15.8 Å<sup>3</sup> and a corresponding density of ρ = 0.97 g/mL. A randomly selected

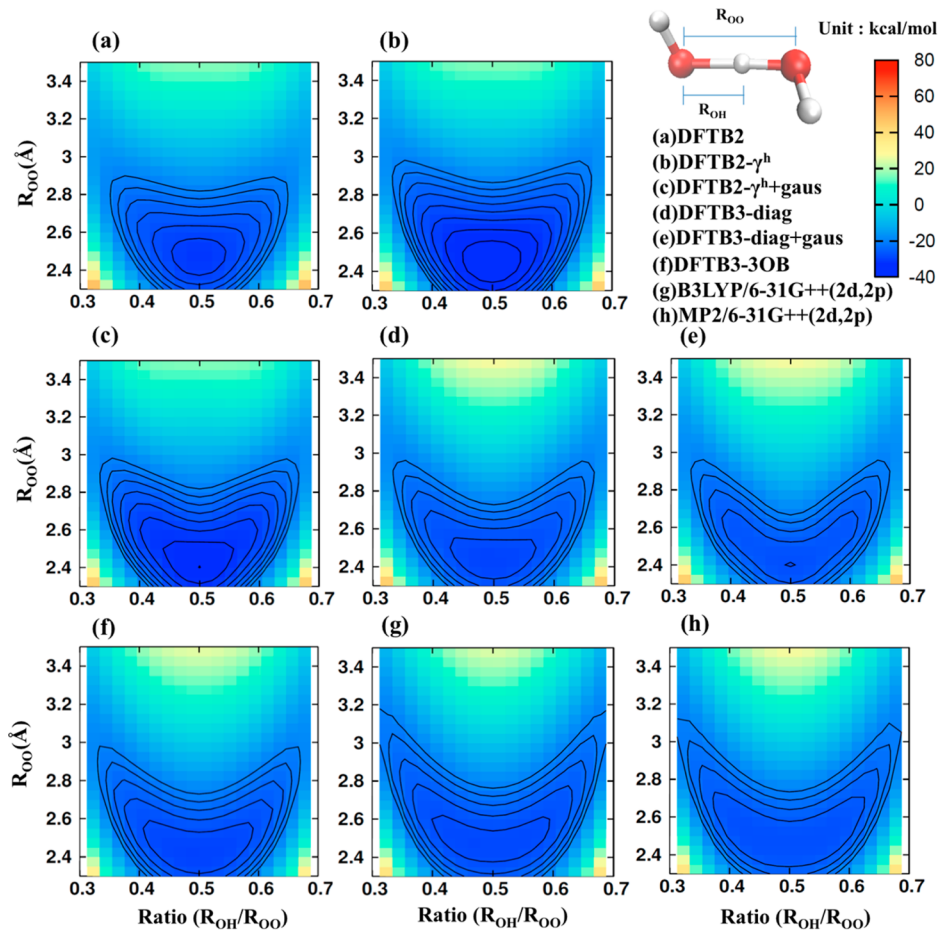


**Figure 1.** Contour plots of  $\text{H}_3\text{O}_2^-$  calculated with various electronic structure methods: (a) DFTB2, (b) DFTB2- $\gamma^h$ , (c) DFTB2- $\gamma^h$ +gaus, (d) DFTB3-diag, and (e) DFTB3-diag+gaus, (f) DFTB3-3OB, (g) B3LYP/6-31G+(2d,2p), and (h) MP2/6-31G+(2d,2p) levels of theory. The difference between two contour lines is 2 kcal/mol.

water molecule from the previous simulations was replaced with a hydroxide anion. This newly created hydroxide system was then duplicated and two 60 ps equilibration runs in the constant NVT ensemble were simulated in each of the various DFTB+ codes.<sup>40</sup> The latter simulations were conducted at a temperature of 300 K using an Anderson thermostat, an integration time step of 1 fs, and an SCC convergence criteria of  $10^{-6}$  atomic units. After equilibration, the systems were subjected to production runs of 50–100 ps in the constant NVE ensemble. The electrostatics for all of the DFTB+ simulations were treated by the supercell sampling using  $2 \times 2 \times 2$  Monkhorst-Pack scheme.<sup>41</sup> In the SCC-DFTB simulations,  $\zeta$  in the modified function in eq 2 was set to 4.5 for the DFTB2- $\gamma^h$  method and 4.95 for DFTB3-diag and DFTB3-diag+gaus methods, as indicated in previous work.<sup>20</sup> For DFTB3-Full+gaus method, the values for  $\zeta$  and Hubbard derivatives  $U^d$  were taken from Table 2 “DFTB3 fit” entry in ref 21. For the DFTB3-3OB calculations the parameters were taken from Table 1 in ref 34.

### 3. RESULTS AND DISCUSSION

**3.1. Potential Energy Surface of  $\text{H}_3\text{O}_2^-$ .** Figure 1 shows the potential energy contour diagrams for  $\text{H}_3\text{O}_2^-$  system using several different electronic structure calculations. In generating the potential energy surfaces, the geometry for the  $\text{H}_3\text{O}_2^-$  cluster was optimized at the MP2/6-31G++(2d,2p) level of theory. The potential energy surface was then created by

scanning the H between OH and  $\text{H}_2\text{O}$  at fixed OO distances. This scanning calculation was repeated by increasing the OO distance by 0.05 Å from 2.0 to 3.5 Å. Other bond lengths and angles were fixed with the optimized geometry during scanning energies. In Figure 1, the y axis represents the OO distance between two oxygen atoms, and the x axis depicts the distance ratio,  $R_{\text{OH}}/R_{\text{OO}}$ , between the OH and OO distance, which indicates the “Zundel” or “Eigen” like hydroxide structures effectively.<sup>42,43</sup>

The shapes of the potential energy surfaces of the DFTB2 (a) and DFTB2- $\gamma^h$  (b) methods are very similar, but the potential energy depth in DFTB2- $\gamma^h$  is about 4 kcal/mol deeper than that in DFTB2. (Eight contour lines in DFTB2- $\gamma^h$  (b), but only six lines in DFTB2 method (a)) These potential shapes are significantly different from those obtained from the B3LYP (f) or MP2 methods (g), which possess a much broader valley near the minima located at about 0.45 and 0.55 Å regions. When the on-site third order correction is included (d and e), the potential shapes become more similar to those of high level electronic structure calculations. The potential energies including the O–H repulsive correction (c and e) indicate a change in the overall surface especially when the hydrogen is located between two oxygen atoms because this O–H repulsive potential was designed to avoid perturbing hydrogen-bonding energies in the barrier region. This correction provides a better description of the proton transfer barrier, but the total potential surface appears distorted when compared to high level

calculations. The potential energy surface calculated with the 3OB parameter set (*f*) is similar to the DFTB3-diag potential, but has a broader curvature in the minimum potential area. Overall, the potential energy surface of the DFTB3-3OB method shows the best contour shape of the  $\text{H}_3\text{O}_2^-$  cluster among all the SCC-DFTB potentials compared to that of the MP2 calculation.

### 3.2. Hydroxide Water Clusters $\text{OH}^-(\text{H}_2\text{O})_n$ , $n = 4-7$ .

The low-lying energy minima of  $\text{OH}^-(\text{H}_2\text{O})_n$ ,  $n = 4-7$ , was evaluated using basin hopping Monte Carlo simulations. In the Appendix, the relative energies of the low-lying local minima of  $\text{OH}^-(\text{H}_2\text{O})_n$ ,  $n = 4-7$ , determined by using the DFTB2- $\gamma^h$  potentials, are given. Several low-lying energy minima were selected, then reoptimized with the MP2/6-31G++(2d,2p) level of theory. These structures are displayed in Figure 2 for

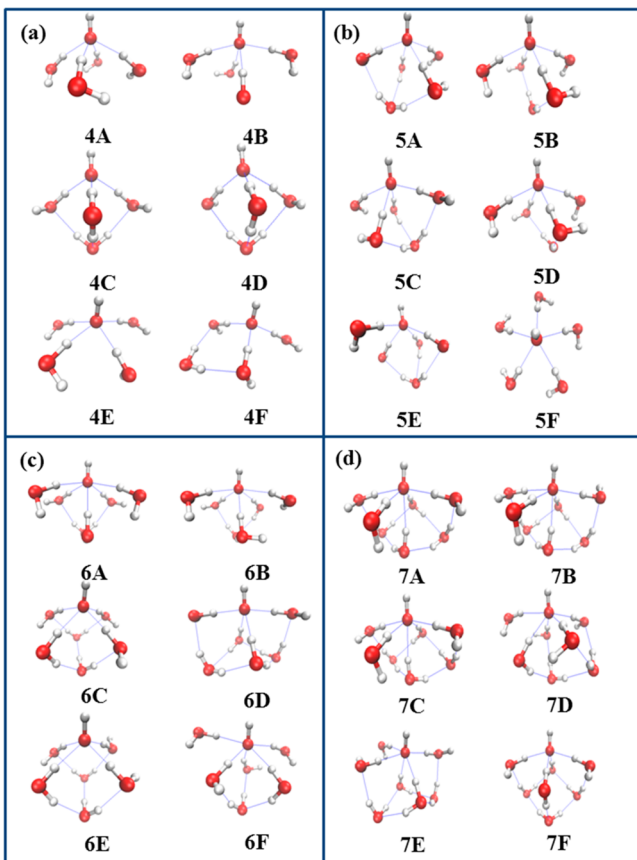


**Figure 2.** Structures of the low-lying energy minima of (a)  $\text{OH}^-(\text{H}_2\text{O})_4$ , (b)  $\text{OH}^-(\text{H}_2\text{O})_5$ , (c)  $\text{OH}^-(\text{H}_2\text{O})_6$ , and (d)  $\text{OH}^-(\text{H}_2\text{O})_7$ . Geometries are optimized with the MP2/6-31G+(2d,2p) level of theory.

$\text{OH}^-(\text{H}_2\text{O})_n$ ,  $n = 4-7$ , and Table 1 shows the formation energies of these small hydroxide water clusters using several different electronic structure calculations. Contrasted to the protonated water clusters, most low-lying minima of the small hydroxide water clusters do not have Zundel-like structures. There are some Zundel-like structures in  $\text{OH}^-(\text{H}_2\text{O})_4$  in Figure 2, calculated with the DFTB2- $\gamma^h$  potential, but these structures (4C and 4D) collapsed back to Eigen-like structures. Table 1 also indicates the lowest energy structure in each electronic structure method (i.e., bold numbers). All the lowest energy structures (4A, 5A, 6A, 7A) are the same in the modified SCC-DFTB methods (DFTB2- $\gamma^h$ , DFTB2- $\gamma^h$  +gaus, DFTB3-diag

+gaus, and DFTB3-diag+gaus and DFTB3-3OB). However the original SCC-DFTB method (DFTB2) shows different lowest energy structures, 4E and 7C, for the  $\text{OH}^-(\text{H}_2\text{O})_4$  and  $\text{OH}^-(\text{H}_2\text{O})_7$  clusters, respectively. This observation indicates the hydrogen-bonding correction (- $\gamma^h$ ) is of significant magnitude to alter the energetics of low-lying energy structures for the small hydroxide water clusters.

The low-lying energy structures calculated with the DFTB methods were reoptimized with the B3LYP and MP2 level of theory. It was found that the minimum energy structures are changed for the  $\text{OH}^-(\text{H}_2\text{O})_n$  clusters,  $n = 4, 6$ , and  $7$ . Only the  $\text{OH}^-(\text{H}_2\text{O})_5$  cluster shows the same minimum structure (5A) for all electronic structure calculations. Table 1 also presents the root-mean-square deviations (rmsd) relative to the MP2 energies for all the clusters. Thus, for the relative energies of these small clusters, the use of third order correction with either MIO or 3OB parameter set does not result in the best accuracy for the  $\text{OH}^-(\text{H}_2\text{O})_n$  cluster,  $n = 4, 6$ , and  $7$ , compared to high level QM calculations. In fact, the incorporation of the third order term results in a less accurate method than the DFTB2 and DFTB2- $\gamma^h$  methods. It is also found that the O-H repulsive correction (+gaus) typically does not change the energy or the structures in these particular cluster calculations because the modified O-H repulsive correction usually affects the structures in the barriers, not in the minima.

While the low-lying energy minimum structures of  $\text{OH}^-(\text{H}_2\text{O})_4$  accept three or four hydrogen-bonds (HBs), those of the  $\text{OH}^-(\text{H}_2\text{O})_n$ ,  $n = 5-7$ , clusters coordinate four or five HBs. Typically tetra-coordinated structures around  $\text{OH}^-$  are observed in the lowest-energy minima of the cluster ( $n \geq 4$ ) when calculated with B3LYP and MP2 levels of theory. The SCC-DFTB method therefore tends to over coordinate the HBs around the  $\text{OH}^-$  anion when compared to high level electronic structure calculations.

**3.3. Hydroxide Bulk Simulations. 3.3.1. Structural Properties.** For the following discussions pertaining to the structural and dynamical properties of the hydrated hydroxide ion it is beneficial to describe the contributing molecules as outlined in Figure 3, which is a typical snapshot from a DFTB2- $\gamma^h$  simulation. In Figure 3, the oxygen and hydrogen of the central hydroxide are denoted as  $\text{O}_0$  and  $\text{H}'$ , respectively. Due to the dynamical nature of the bonding topology and solvent environment, the first solvation shell has been included in the description of the central hydroxide. The oxygen atoms on the surrounding waters are denoted in general as  $\text{O}_w$ . The nearest solvating waters are denoted as  $\text{O}_1$ ,  $\text{O}_2$ ,  $\text{O}_3$ , ...,  $\text{O}_n$ , as determined by the distance between  $\text{O}_0$  and the surrounding water oxygens. In this section, the structural properties predicted by the various DFTB methods are compared with the structural properties predicted by the CPMD results,<sup>4,5</sup> which are consistent with known experimental data in terms of both structural and dynamical properties.

The radial distribution function (RDF) between the hydroxide's oxygen ( $\text{O}_0$ ) and the surrounding water oxygens ( $\text{O}$ ) can be found in Figure 4A. Evaluation of the first peak's location indicates that the various SCC-DFTB methods predict the first solvation shell to reside at  $R_{\text{O}_0-\text{O}} = 2.68 \pm 0.01 \text{ \AA}$ , larger than the CPMD result, which predicts  $R_{\text{O}_0-\text{O}} = 2.6 \text{ \AA}$ . This suggests that in bulk water, the SCC-DFTB methods overestimate the distance between hydroxide ion and its first solvation shell by nearly 0.1  $\text{\AA}$ . In addition, the first peak predicted by SCC-DFTB is much narrower than that in

Table 1. Formation Energies (kcal/mol) of Several Isomers of  $\text{OH}^-(\text{H}_2\text{O})_n$ , for  $n = 4-7$ 

$\text{OH}^-(\text{H}_2\text{O})_4$	DFTB2	DFTB2- $\gamma^h$	DFTB2- $\gamma^h$ +gaus	DFTB3-diag	DFTB3-diag+gaus	DFTB3-3OB	B3LYP/6-31G++(2d,2p)	MP2/6-31G++(2d,2p)
4A	-81.78	<b>-95.22<sup>b</sup></b>	-95.22	-95.14	-95.14	-91.13	-84.42	-87.55
4B	-80.82	-94.78	-94.78	-94.41	-94.41	-90.09	-83.22	-85.16
4C	-80.58	-94.51	-94.40	-93.30	-93.30	-88.83	-85.12	<b>-87.85</b>
4D	-80.39	-94.27	-92.52	-91.86	-89.64	-88.32	-84.66	-87.30
4E	<b>-81.82</b>	-94.16	-94.14	-94.41	-94.41	-90.09	-83.22	-85.53
4F	-80.83	-93.54	-93.53	-89.08	-89.08	-86.62	<b>-85.16</b>	-86.48
rmsd <sup>a</sup>	1.28	1.05	1.43	2.68	3.20	2.16	0.98	0
$\text{OH}^-(\text{H}_2\text{O})_5$	DFTB2	DFTB2- $\gamma^h$	DFTB2- $\gamma^h$ +gaus	DFTB3-diag	DFTB3-diag+gaus	DFTB3-3OB	B3LYP/6-31G++(2d,2p)	MP2/6-31G++(2d,2p)
5A	<b>-94.93</b>	<b>-111.90</b>	-111.90	<b>-112.46</b>	<b>-112.46</b>	<b>-105.56</b>	<b>-99.01</b>	<b>-103.68</b>
5B	-94.55	-111.21	-111.21	-111.52	-111.52	-104.08	-97.60	-102.08
5C	-94.22	-110.90	-110.90	-110.98	-110.98	-104.68	-98.41	-102.98
5D	-94.56	-110.97	-110.97	-111.17	-111.17	-104.64	-98.36	-102.88
5E	-94.27	-110.43	-110.43	-110.48	-110.48	-103.01	-97.23	-101.45
5F	-94.76	-109.81	-109.81	-109.36	-109.36	-103.63	-94.97	-99.69
rmsd <sup>a</sup>	1.64	0.92	0.92	0.60	0.60	0.86	0.22	0
$\text{OH}^-(\text{H}_2\text{O})_6$	DFTB2	DFTB2- $\gamma^h$	DFTB2- $\gamma^h$ +gaus	DFTB3-diag	DFTB3-diag+gaus	DFTB3-3OB	B3LYP/6-31G++(2d,2p)	MP2/6-31G++(2d,2p)
6A	<b>-107.77</b>	<b>-127.50</b>	-127.50	<b>-129.41</b>	<b>-129.41</b>	<b>-119.97</b>	-110.34	-116.85
6B	-107.07	-126.51	-126.51	-128.37	-128.37	-119.26	-111.02	-116.08
6C	-107.19	-125.91	-125.88	-126.74	-126.74	-117.98	<b>-113.55</b>	<b>-119.52</b>
6D	-106.64	-125.94	-125.94	-127.51	-127.51	-117.78	-112.13	-118.01
6E	-106.66	-125.56	-125.54	-125.62	-125.62	-117.65	-113.18	-119.04
6F	-106.45	-125.32	-125.32	-126.53	-126.53	-117.37	-113.55	-114.69
rmsd <sup>a</sup>	1.98	2.67	2.68	3.52	3.52	2.98	2.31	0
$\text{OH}^-(\text{H}_2\text{O})_7$	DFTB2	DFTB2- $\gamma^h$	DFTB2- $\gamma^h$ +gaus	DFTB3-diag	DFTB3-diag+gaus	DFTB3-3OB	B3LYP/6-31G++(2d,2p)	MP2/6-31G++(2d,2p)
7A	-119.33	<b>-141.18</b>	<b>-141.18</b>	<b>-143.73</b>	<b>-143.73</b>	<b>-132.22</b>	-123.96	-131.67
7B	-119.12	-141.12	-141.12	-143.97	-143.97	-131.74	-123.16	-130.79
7C	<b>-119.36</b>	-141.11	-141.11	-143.73	-143.73	-132.14	-123.79	-131.57
7D	-118.93	-140.74	-140.74	-143.38	-143.38	-131.76	-125.37	-131.63
7E	-118.72	-140.36	-140.36	-143.06	-143.06	-131.72	-126.56	-130.51
7F	-118.17	-139.76	-138.03	-140.33	-138.20	-130.25	<b>-127.05</b>	<b>-134.13</b>
rmsd <sup>a</sup>	1.41	1.63	2.32	2.45	3.30	1.85	1.67	0

<sup>a</sup>rmsd given relative to the MP2 energies. <sup>b</sup>The bold number indicates the lowest energy structure in each method.

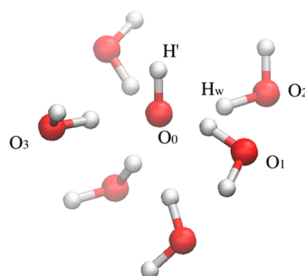


Figure 3. Solvation of the hydroxide anion in bulk water. The hydroxide oxygen and hydrogen are labeled as  $O_0$  and  $H'$ , respectively. The nearest three surrounding water oxygens are labeled as  $O_1$ ,  $O_2$ , and  $O_3$ . The water hydrogen is labeled as  $H_w$ .

CPMD, which indicates that SCC-DFTB methods predict a more ordered first solvation shell around the hydroxide ion in bulk water as compared to CPMD.

The oxygen coordination number of the central hydroxide, which indicates the number of solvating waters, can be determined by integrating the first peak of RDF of  $O_0-O$  for the SCC-DFTB and CPMD data:

$$n = 4\pi\rho \int_{r_1}^{r_2} r^2 g_{O_0-O}(r) dr \quad (6)$$

where  $n$  is the oxygen coordination number,  $\rho$  is the bulk density of water oxygen, and  $r_1$  and  $r_2$  are the starting and

ending radial distance of the first peak, respectively. The results of the first peak integration and first peak height are found in Table 2. From Table 2, it is obvious that the coordination numbers predicted by the various SCC-DFTB methods are much larger than the CPMD result. This indicates that the SCC-DFTB methods have a tendency to oversolvate the hydroxide ion. The oversolvation of the hydrated hydroxide ion is similar to what the cluster calculations predict and have also been seen in both the evaluation of the hydrated excess proton and the bulk water characteristics as described by the SCC-DFTB method.<sup>19</sup>

The structural information in Figure 4 and Table 2 indicates that from DFTB2 to DFTB3-diag, the progressive addition of correction term to the SCC-DFTB description of the hydroxide ion has the major effect of increasing the height of the first peak as well as the coordination number in the first solvation shell for the hydroxide ion. It is found that the DFTB2- $\gamma^h$  causes slight oversolvation of hydroxide with respect to the DFTB2, which has the best agreement with CPMD data. The increase in the first peak height and coordination number caused by the  $\gamma^h$  function is in line with the increased depth of in the potential energy surface for  $\text{H}_3\text{O}_2^-$  cluster, as already mentioned in section 3.1 (Figure 1a and b). The enhanced  $\text{OH}^-\text{-H}_2\text{O}$  dimer interaction energy predicted by DFTB2- $\gamma^h$  is responsible for a more structured first solvation shell compared to DFTB2. The addition of the O-H repulsive potential to DFTB2- $\gamma^h$  causes a

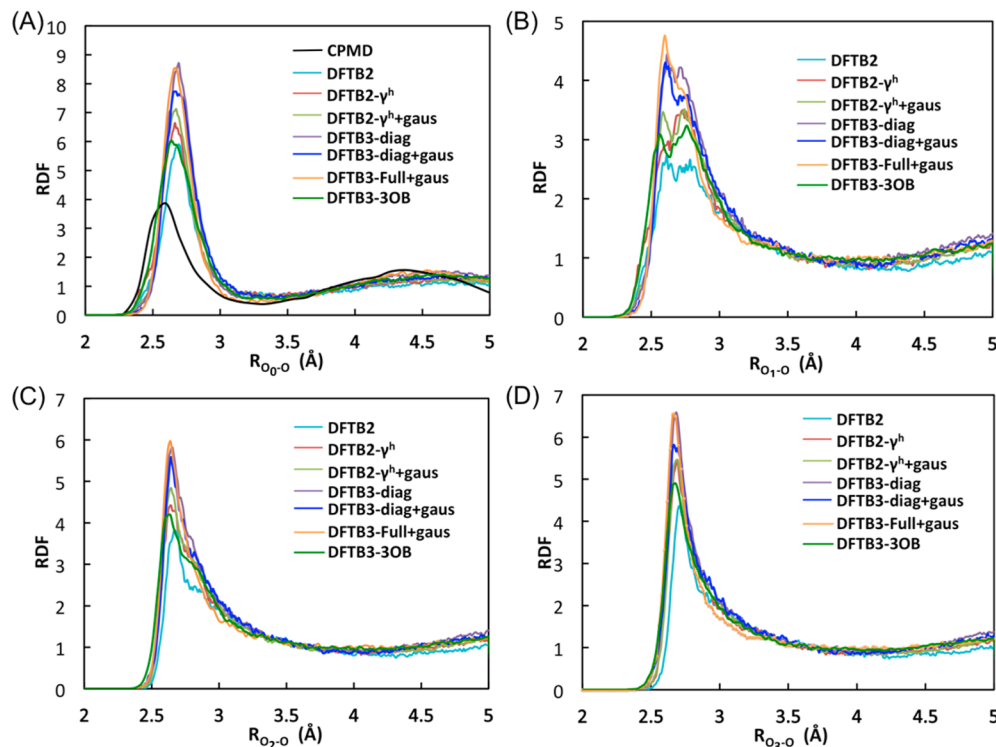


**Figure 4.** Radial distribution functions of the hydroxide anion complex for (A)  $g_{O_0-O}(r)$ , (B)  $g_{O_1-O}(r)$ , (C)  $g_{O_2-O}(r)$ , and (D)  $g_{O_3-O}(r)$  (see Figure 3 for definitions). Each panel has data for DFTB2 (light blue), DFTB2- $\gamma^h$  (red), DFTB2- $\gamma^h$ +gaus (light green), DFTB3-diag (purple), DFTB3-diag+gaus (deep blue), DFTB3-Full+gaus (orange), and DFTB3-3OB (deep green) simulations. For  $g_{O_0-O}(r)$ , CPMD simulation data is shown in black.

**Table 2. Coordination Number of Hydroxide and First Peak Height of  $g_{O_0-O}(r)$**

method	coordination number	first peak height
CPMD <sup>4,5</sup>	4.8	4.5
DFTB2	$6.62 \pm 0.03$	$5.7 \pm 0.2$
DFTB2- $\gamma^h$	$6.87 \pm 0.04$	$6.5 \pm 0.2$
DFTB2- $\gamma^h$ +gaus	$6.94 \pm 0.05$	$6.9 \pm 0.3$
DFTB3-diag	$7.87 \pm 0.04$	$8.68 \pm 0.03$
DFTB3-diag+gaus	$7.82 \pm 0.07$	$7.78 \pm 0.07$
DFTB3-Full+gaus	$7.36 \pm 0.03$	$8.6 \pm 0.1$
DFTB3-3OB	$7.0 \pm 0.1$	$6.07 \pm 0.05$

further slight increase in first peak height and coordination number. The introduction of third order correction terms while using the MIO parameter set has a major adverse impact on the solvation structure as compared to the CPMD simulations. For the three methods DFTB3-diag, DFTB3-diag+gaus and DFTB3-Full+gaus, the first peak height is greatly enhanced and the hydroxide accommodates an additional water molecule in the first solvation shell when compared to the DFTB2 method prediction. Additional changes in the RDF include a narrowing of the first peak and a more pronounced second peak, indicating more ordering in both the first and second solvation shells. The increased over solvation and structuring in the first solvation shell are in line with the increase in the interaction energy of hydroxide clusters for the DFTB3 and DFTB3-diag+gaus methods as compared to the DFTB2 methods (Table 1). It is worth noting that the addition of the repulsive potential to DFTB3-diag method and the use of the full third order correction do not result in significant

improvement, but the use of the 3OB parameter set in the DFTB3-3OB method does generates a better result than the MIO parameter set. The use of the 3OB parameter set reduces the hydroxide oversolvation and makes the solvation shells less ordered, which is in agreement with the decrease in the interaction energy of hydroxide clusters for DFTB3-3OB compared to DFTB3-diag (Table 1). The reason for the improvement may be that the 3OB parameter set is optimized for SCC-DFTB with full third order expansion, but the MIO parameter set was developed for the original DFTB2. However, the DFTB3-3OB method still predicts results qualitatively different from CPMD. Interestingly, the newest state-of-art DFTB3-3OB method provides results with an accuracy only similar to the original DFTB2 methods.

Further analysis of the structural properties requires the inspection of the solvation environment for the first solvation shell around the hydroxide ion. The RDF for O<sub>1</sub>-O (Figure 4B) indicates the presence of a special pair, like that seen for the hydrated excess proton,<sup>19</sup> although to a much smaller extent. In Figure 4B, it is clear that the first peak is more pronounced in the third order methods with MIO parameter set than in the second order method, indicating that with a more ordered solvation environment the presence of a special pair becomes more obvious and localized. The first subpeak in the first main peak is more dominant in DFTB3 with MIO parameter set than the DFTB2 methods, which indicates that the O<sub>1</sub> is more localized (i.e., held tighter to O<sub>0</sub>). Similar to the previously reported trends, the DFTB3-3OB method exhibits an improvement over the DFTB3 methods using the MIO parameter set, providing results similar to the DFTB2 methods.

In the RDF for  $O_2-O$  and  $O_3-O$  (Figure 4C and D), the first peaks are located at  $2.65 \pm 0.01$  and  $2.69 \pm 0.02$  Å, respectively, indicating that there is degeneracy in the distance and preference for a particular water in this solvation shell. The first peak's height and coordination number are listed in Tables 3 and 4 for  $O_2-O$  and  $O_3-O$ , respectively, indicating an

**Table 3. Coordination Number of  $O_2$  and First Peak Height of  $g_{O_2-O}(r)$**

method	coordination number	first peak height
DFTB2	$9.36 \pm 0.08$	$3.7 \pm 0.1$
DFTB2- $\gamma^h$	$10.15 \pm 0.01$	$4.48 \pm 0.08$
DFTB2- $\gamma^h$ +gaus	$10.14 \pm 0.02$	$4.8 \pm 0.1$
DFTB3-diag	$11.12 \pm 0.03$	$5.83 \pm 0.02$
DFTB3-diag+gaus	$10.9 \pm 0.1$	$5.5 \pm 0.1$
DFTB3-Full+gaus	$10.5 \pm 0.1$	$5.99 \pm 0.02$
DFTB3-3OB	$10.31 \pm 0.06$	$4.19 \pm 0.05$

**Table 4. Coordination Number of  $O_3$  and First Peak Height of  $g_{O_3-O}(r)$**

method	coordination number	first peak height
DFTB2	$9.40 \pm 0.08$	$4.3 \pm 0.1$
DFTB2- $\gamma^h$	$10.11 \pm 0.06$	$5.418 \pm 0.002$
DFTB2- $\gamma^h$ +gaus	$10.14 \pm 0.06$	$5.3 \pm 0.2$
DFTB3-diag	$11.10 \pm 0.08$	$6.57 \pm 0.01$
DFTB3-diag+gaus	$10.94 \pm 0.08$	$5.9 \pm 0.1$
DFTB3-Full+gaus	$10.5 \pm 0.1$	$6.6 \pm 0.1$
DFTB3-3OB	$10.26 \pm 0.05$	$4.90 \pm 0.01$

oversolvation behavior. The peak position and starting point of the first peak is observed to shift slightly to the left as one changes the method from DFTB2 to DFTB3-Full+gaus. The peak's height and coordination number reflect the same trend in the RDF of  $O_0-O$  and  $O_1-O$ , revealing an oversolvation and ordering of the waters. The DFTB3 methods using MIO parameter set greatly enhanced the height of the first peak as well as the coordination number compared to DFTB2 methods. These structural changes are due to the overall increased ordering in the solvation structure and number of solvating waters. The DFTB3-3OB reduces these problems and leads to results comparable to DFTB2 methods. It is also obvious that all the SCC-DFTB methods predict a very broad density depletion region between the first and second solvation shell and the depletion is weak in magnitude. This has the impact of causing abnormally large coordination numbers (Table 4) due to the fuzzy cutoff region between solvation shells. The same structural feature was observed in our previous paper for hydrated excess proton system.<sup>19</sup>

To gain more insight into the detailed structure of the first solvation shell of the hydroxide ion, the partial RDFs with reference to  $O_0$  for various DFTB methods are plotted in Figure 5. It is observed that the DFTB3 methods with the MIO parameter set lead to the narrowing of the partial RDF, which is in agreement with the narrowing of the first peak in  $O_0-O$  RDF. Looking at the relative shapes of the subpeaks one can see that as the peaks move farther away from the hydroxide they increase in width. This is indicative of waters that associate less favorable than closer waters (i.e., reduced interaction energy). However, this trend is not pronounced for the DFTB3 methods with the MIO parameter set, again indicating the stronger interaction between the hydroxide ion and the

surrounding waters. Closer inspection of Figure 5 reveals that those DFTB3 method's subpeaks are packed closer to each other than DFTB2 methods, indicating a tighter and closer solvation shell with reduced movements and fluctuations. These observations are in agreement with our earlier conclusions that the DFTB3 methods with the MIO parameter set have a more ordered structure in the first solvation shell. The DFTB3-3OB method leads to a less structured first solvation shell and provides similar results to the DFTB2 methods.

Overall, the variety of hydroxide oxygen–oxygen RDF's indicate that the DFTB3 methods with the MIO parameter set make the solvation structure more ordered and densely packed in regions near the hydroxide ion, which may exacerbate the observed “water voids” issue (see section 3.5). It is found that the DFTB3 methods with the MIO parameter set generate results more at odds with those of the CPMD calculation than the results generated with the DFTB2 methods, while the DFTB3-3OB method is found to be a modest improvement over the MIO parameter set.

In addition to analyzing the oxygen–oxygen structures it is also beneficial to inspect the hydrogen–oxygen structures and the resulting hydrogen bonding network. The RDF of  $H'-O_w$  are shown in Figure 6A. The  $\delta$  in Figure 6A is a PT reaction coordinate defined<sup>5</sup> as:  $|\delta| = \min|R_{O_aH} - R_{O_bH}|$ , where  $O_a$  is any possible oxygen atom that is involved in a hydrogen bond with the hydroxide, and  $R_{O_aH}$  and  $R_{O_bH}$  are the distances between the shared hydrogen and the two oxygens. A small  $\delta$  correspond to the transition state of the PT reaction, while a large  $\delta$  correspond to the system residing in the reactant or product well (i.e., resting state). The first peak's height from the DFTB3 methods is near 2 and is more pronounced when compared to those of the CPMD methods, which is below 0.8 for both the resting and transition states. Integration over the first peak in the RDF of  $H'-O_w$  for DFTB3-diag, DFTB3-diag+gaus, DFTB3-Full+gaus and DFTB3-3OB gives hydrogen coordination number of  $0.93 \pm 0.02$ ,  $0.86 \pm 0.01$  and  $0.93 \pm 0.03$ ,  $0.83 \pm 0.02$ , respectively, larger than the value of 0.72 predicted by CPMD simulation.<sup>4</sup> It is also observed that the positions of the RDF's first peaks for the DFTB3 methods are shifted to smaller separation distances as compared to the DFTB2 methods. This indicates that the DFTB3 methods strengthen the hydrogen bond donated by the hydroxide to the nearby water oxygen, and for the majority of the simulation time the hydroxide hydrogen is hydrogen bonded to a water molecule's oxygen, which is in sharp contrast with CPMD conclusions.<sup>4,5</sup> This hydrogen accepting water molecule accounts for the additional water molecule solvating the hydroxide as compared to the DFTB2 methods. The DFTB3-3OB method slightly reduces the coordination number and the peak height, but is still qualitatively different from DFTB2 and CPMD results, suggesting that the 3OB parameter set does not significantly improve the hydrogen bonding interaction between water and the hydroxide ion.

The RDF for the central oxygen,  $O_0-H$ , is shown in Figure 6B, and the integration of the second peak is the hydrogen coordination number for the hydroxide oxygen as depicted in Table 5. The second peaks for the various SCC-DFTB methods reside at  $1.70 \pm 0.02$  Å, whereas the CPMD simulations predict 1.6 Å, indicating a slight elongation of the oxygen hydrogen distance for the SCC-DFTB methods. This suggests that the SCC-DFTB methods predict a larger donating hydrogen bond

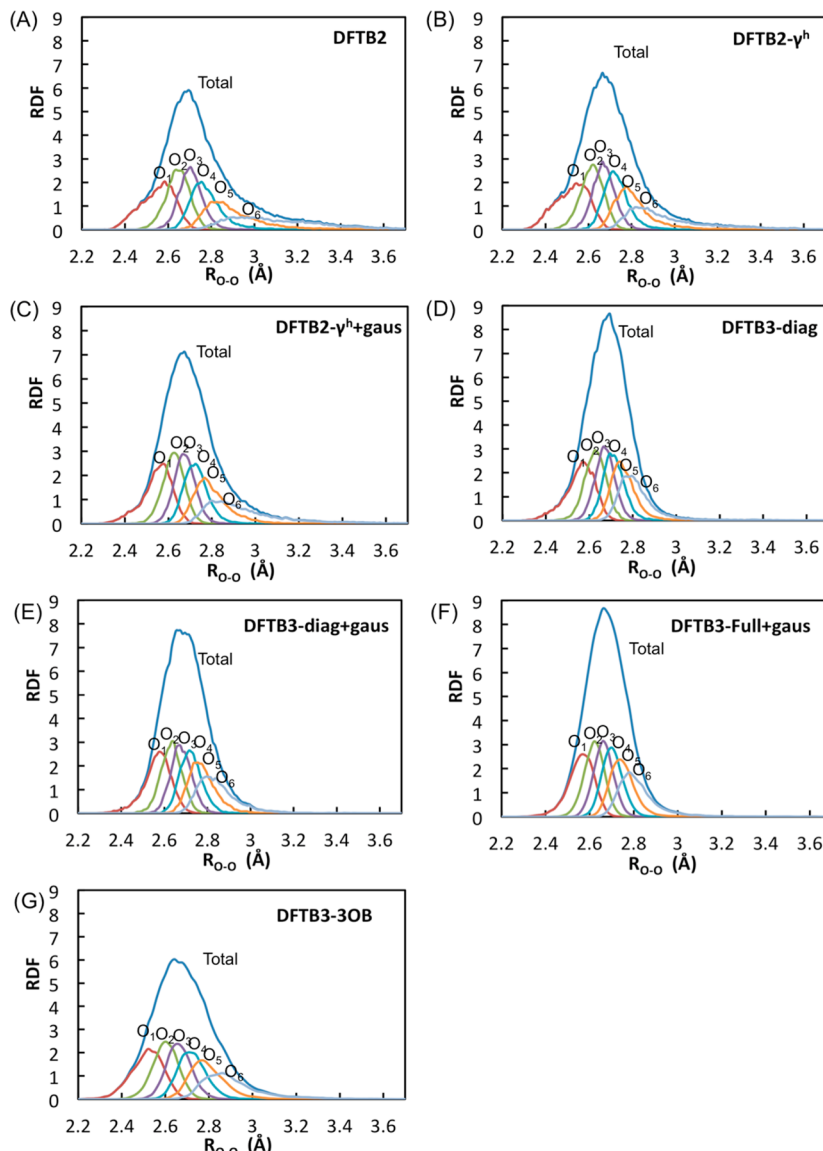


**Figure 5.** Partial radial distribution function for the six nearest waters to the hydroxide for (A) DFTB2, (B) DFTB2- $\gamma^h$ , (C) DFTB2- $\gamma^h+gaus$ , (D) DFTB3-diag, (E) DFTB3-diag+gaus, (F) DFTB3-Full+gaus, and (G) DFTB3-3OB simulations. The notation for “ $O_1$ ”, “ $O_2$ ”, “ $O_3$ ”, etc. stands for partial RDF of  $O_0-O_1$ ,  $O_0-O_2$ ,  $O_0-O_3$ , etc..

length, and is in line with the observation from the RDF of  $O_0-O$  that reveals the distance between the hydroxide ion and its first solvation shell to be about 0.1 Å larger in SCC-DFTB than in CPMD. The use of the 3OB parameter set does not result in an appreciable change in the location of the second peak, which again suggests that it fails to significantly improve the description of hydrogen bonds between water and hydroxide. Moreover, the second peak width in RDF of  $O_0-H$  in SCC-DFTB methods is narrower than that in CPMD simulation, again suggesting a more ordered solvation shell. In addition, the SCC-DFTB methods appear to have an overall tendency to donate more hydrogen bonds to the central hydroxide oxygen, and as observed from the hydrogen coordination number, the hydroxide does not accept more hydrogen bonds from the first solvation shell waters in the DFTB3 methods as compared to DFTB2 methods. This is in agreement with the observation from the RDF of  $H'-O_w$ , which indicates that the additional solvating water in the DFTB3 methods is accepting hydrogen bonds from the hydroxide rather than donating hydrogen

bonds. Although the hydrogen coordination numbers are similar for the various SCC-DFTB methods, it is observed that the second peak's height increases significantly in going from DFTB2 methods to DFTB3 methods with MIO parameter set, again indicating an increased ordering and localization of atoms around the hydroxide ion. The DFTB3-3OB again reduces the degree of over structuring, providing similar results to the DFTB2 methods.

In addition, from the comparison between DFTB2- $\gamma^h$  vs DFTB2- $\gamma^h+gaus$ , and DFTB3-diag vs DFTB3-diag+gaus, we can see the shoulders in the second peak are reduced when the  $O-H$  repulsive potential is added. This indicates that the  $O-H$  repulsive potential creates a density depletion area that is unfavorable for the surrounding waters hydrogen atoms to enter. The absence of hydrogen density in the shoulder area is in line with the effect of the  $O-H$  repulsive potential in the region from 1–1.5 Å. It is important to note that the absence of the shoulder region in the second peak is also seen in CPMD simulations.<sup>45</sup>

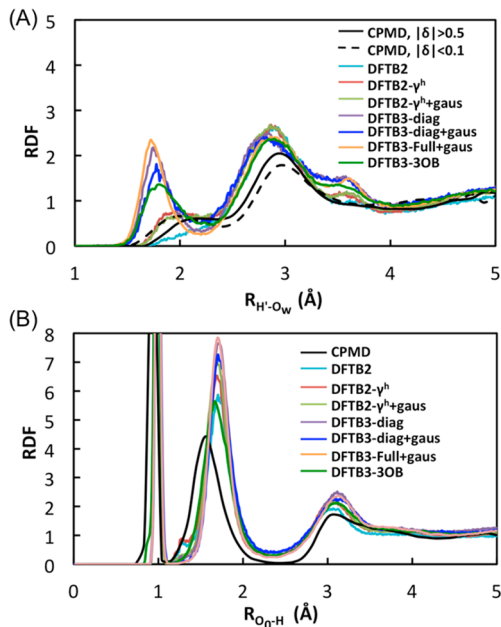


**Figure 6.** Radial distribution functions of the hydroxide anion complex for (A)  $g_{H'-O_w}$  and (B)  $g_{O_0-H}(r)$ . Each panel has data for DFTB2 (light blue), DFTB2- $\gamma^h$  (red), DFTB2- $\gamma^h$ +gaus (light green), DFTB3-diag (purple), DFTB3-diag+gaus (deep blue), DFTB3-Full+gaus (orange), and DFTB3-3OB (deep green) simulations. CPMD simulation data is shown in black.

**Table 5. Coordination Number of Hydrogen and Second Peak Height for  $g_{O_0-H}(r)$**

method	coordination number	second peak height
CPMD <sup>4,5</sup>	4.0	4.5
DFTB2	$5.02 \pm 0.06$	$5.7 \pm 0.2$
DFTB2- $\gamma^h$	$5.35 \pm 0.07$	$6.4 \pm 0.1$
DFTB2- $\gamma^h$ +gaus	$5.47 \pm 0.08$	$6.8 \pm 0.3$
DFTB3-diag	$5.98 \pm 0.05$	$7.7 \pm 0.1$
DFTB3-diag+gaus	$5.8 \pm 0.1$	$7.1 \pm 0.2$
DFTB3-Full+gaus	$5.60 \pm 0.01$	$7.9 \pm 0.1$
DFTB3-3OB	$5.26 \pm 0.04$	$5.6 \pm 0.1$

A closer examination of Figure 3, a typical snapshot from the DFTB2- $\gamma^h$  method, provides useful clues as to the origin of the oversolvation of the hydroxide ion. In the dynamical hypercoordination scenario of the CPMD simulations,<sup>4,5</sup> the hydroxide accepts four hydrogen bonds from four surrounding waters in a nearly square planar arrangement (Figure 1e in ref 4). However, in the DFTB2- $\gamma^h$  method, in addition to the 4 hydrogen-donating waters arranged in a roughly planar structure, there are two more waters donating hydrogen bonds from below the square planar structural plane. These two waters account for the oversolvation trend of the hydroxide ion by the SCC-DFTB methods. The increased number of hydrogen bonds in the DFTB methods compared to CPMD method is also in agreement with the  $\text{OH}^-(\text{H}_2\text{O})_n$  cluster simulation result mentioned in section 3.2 and the conclusions from the RDF of  $\text{O}_0-\text{H}$ . As will be discussed in the next sections, this oversolvation causes incorrect energetic and dynamical properties of the hydroxide hopping.

**3.3.2. Energetic Properties.** In Figure 7, the potential of mean force (PMF) for the transfer of a proton along the

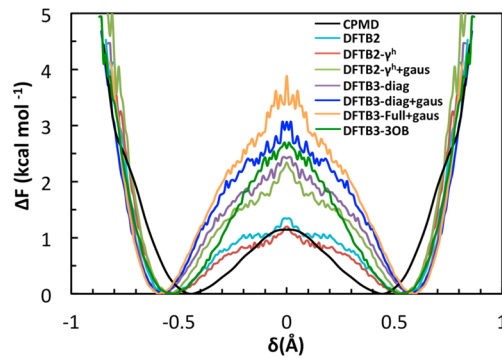


**Figure 7.** Potential of mean force for the hydroxide for proton transport in  $\text{H}_3\text{O}_2^-$  for CPMD (black), DFTB2 (light blue), DFTB2- $\gamma^h$  (red), DFTB2- $\gamma^h$ +gaus (light green), DFTB3-diag (purple), DFTB3-diag+gaus (deep blue), DFTB3-Full+gaus (orange), and DFTB3-3OB (deep green) simulations. The potential of mean force is represented as a function of the  $\delta$  coordinate described in the text.

reaction coordinate  $\delta$ , described above, in various DFTB methods are depicted. The PMF is calculated as

$$F = -k_B T \ln P(\delta) \quad (7)$$

where  $P(\delta)$  is the probability that a certain value of  $\delta$  is observed during the MD run.

From Figure 7, the following observations are made:

1. All the SCC-DFTB methods predict a larger minima  $\delta$  value for the PMF. The larger minima  $\delta$  value predicted by SCC-DFTB can be explained by the larger separation between hydroxide ion and its surrounding water molecules in SCC-DFTB compared to CPMD simulations. This result is in line with the conclusions drawn from the RDFs for  $\text{O}_0-\text{O}$  and  $\text{O}_0-\text{H}$ .
2. The DFTB2 and DFTB2- $\gamma^h$  methods give similar PT energy barriers compared to the CPMD value,  $\Delta E \approx 1.15 \text{ kcal/mol}$ .<sup>4,5</sup> However, the addition of the on-site third order correction raises hydroxide hopping barrier by at least 1 kcal/mol, and the addition of the full third order correction raises the barrier even more. This behavior indicates that the PT will be less pronounced in the DFTB3 results than in the DFTB2 results. The reduction in the hydroxide transport is caused by the extreme oversolvation of the hydroxide and the large energy required to reorganize the hydrogen bond network topology during PT. The DFTB3-3OB method improves the results over the MIO parameter set and reduces the barrier to 2.5 kcal/mol, but it is still higher than the DFTB2 methods, which are in better agreement with the CPMD results.
3. The addition of the O–H repulsive potential raises the barrier height for hydroxide transfer thereby favoring the resting state (i.e., product and or reactant). The hydroxide hopping barrier is raised by about 1 kcal/mol from DFTB2- $\gamma^h$  to DFTB2- $\gamma^h$ +gaus and by about 0.5 kcal/mol from DFTB3-diag to DFTB3-diag+gaus. These observations indicate that the transition state for hydroxide hopping is disfavored in the DFTB2- $\gamma^h$ +gaus and DFTB3-diag+gaus results. This is due to the fact that when the donating proton reaches the hopping region where  $|\delta|$  approaches zero, the proton is interacting with the Gaussian repulsive potential in an unfavorable

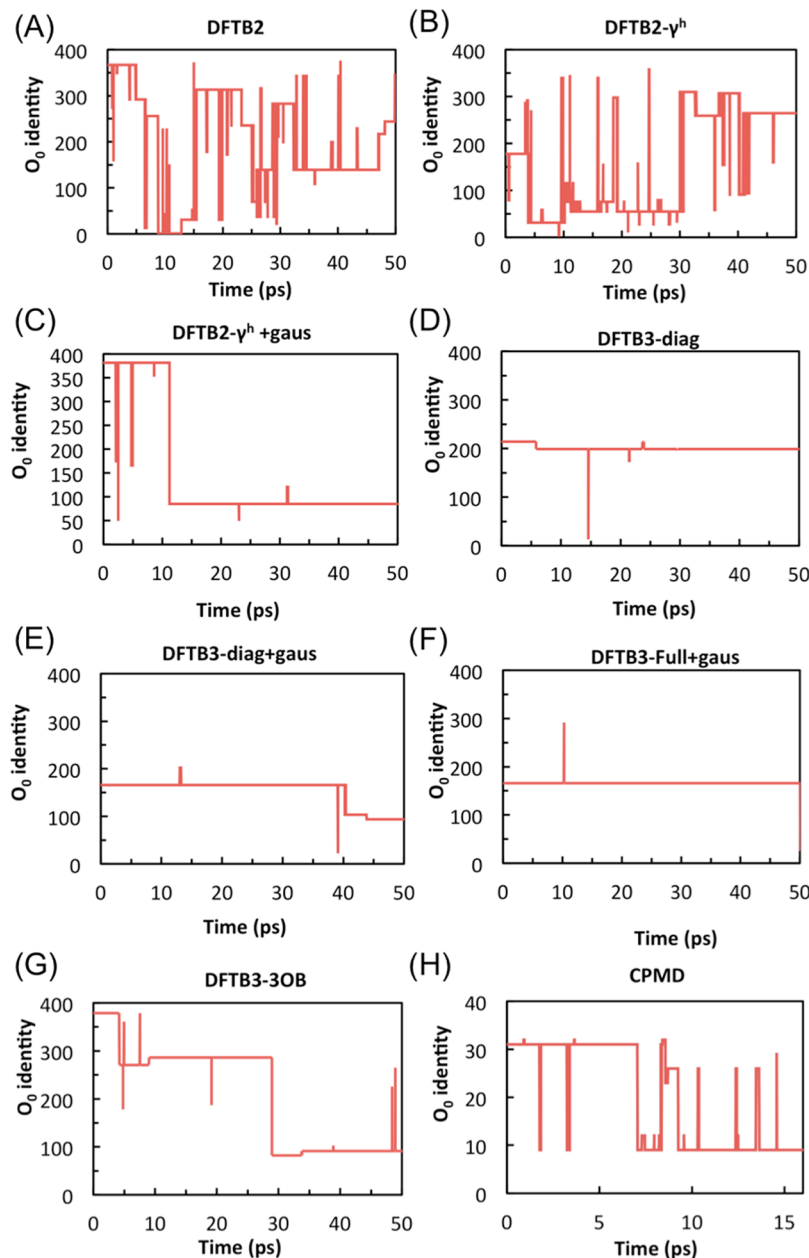


**Figure 8.** Time dependence of the identity of  $O_0$  for the (A) DFTB2, (B) DFTB2- $\gamma^h$ , (C) DFTB2- $\gamma^h$ +gaus, (D) DFTB3-diag, (E) DFTB3-diag+gaus, (F) DFTB3-Full+gaus, (G) DFTB3-3OB, and (H) CPMD simulations. The data depicted here is for one of the two independent trajectories. The reader should note the differences in scale of the horizontal axis between the various panels of the figure.

fashion. Therefore, the “reverse” Grotthuss hopping is energetically disfavored. The increased hopping barrier caused by the O–H repulsive potential is also in accordance with the recent report from Goyal et al. (ref 20) for the hydrated proton in water. The incorrect free energy profiles predicted by SCC-DFTB methods result in incorrect hydroxide hopping dynamical properties, which we discuss below.

**3.3.3. Dynamical Properties.** For each SCC-DFTB version, the hydroxide oxygen’s identity was followed during the MD simulation to gain insight into the mechanism for hydroxide transport. The results of the hydroxide identity are plotted in Figure 8. The DFTB2 and DFTB2- $\gamma^h$  methods give similar frequency for identity change of  $O_0$  as that predicted in the dynamical hypercoordination scheme in previous CPMD

simulations.<sup>4,5</sup> The thick line region for the DFTB2 methods is slightly more pronounced than that found for the CPMD simulations, indicating a longer oscillatory shuttling, where the proton is transferred back and forth between the same two oxygen atoms. It is clear from Figure 8C and E that the O–H repulsive potential has a deleterious effect on the hopping rate. As mentioned in the free energy analysis, this is because the repulsive potential tends to disfavor the hydrogen located at the midpoint of two sharing oxygens. The overall result is a significant reduction in the number of successful hopping events and a resulting model that favors vehicular (standard diffusive) transport over the Grotthus type bond rearrangement-process.

Evaluation of the DFTB3 methods with the MIO parameter set clearly reveals a greatly suppressed Grotthuss hopping

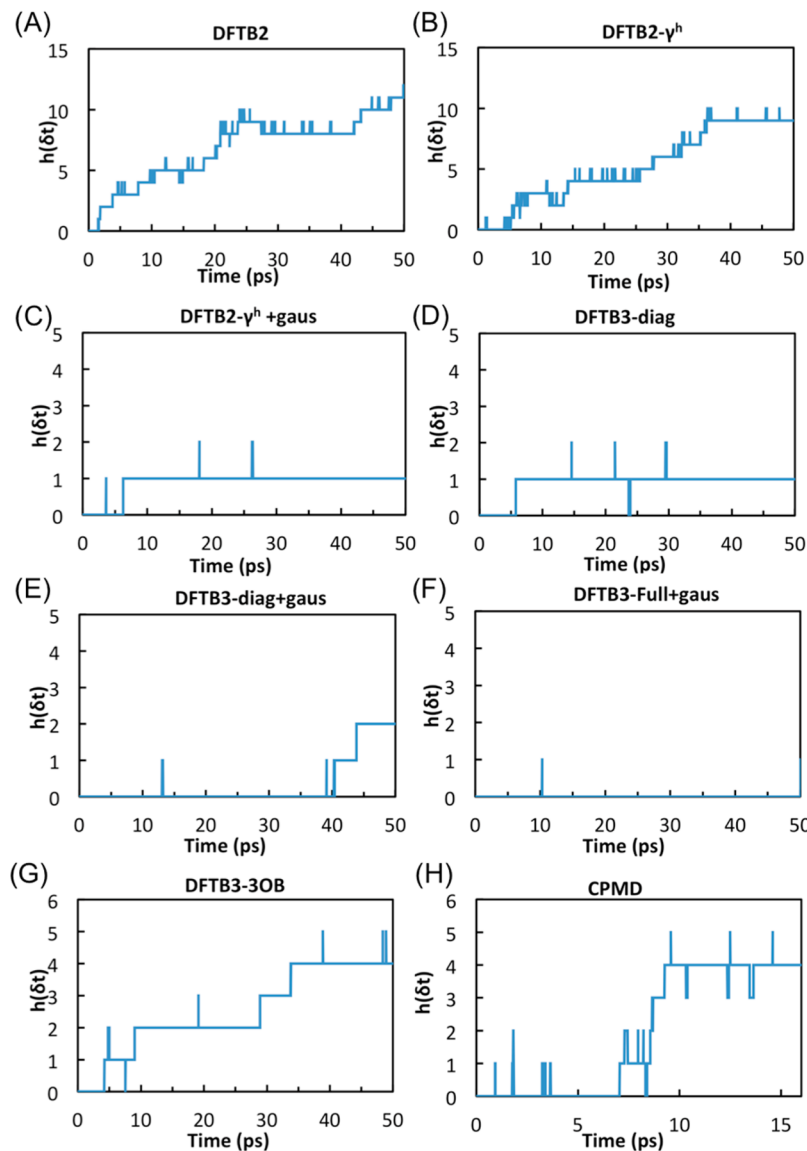


**Figure 9.** Forward proton hopping function calculated from (A) DFTB2, (B) DFTB2- $\gamma^h$ , (C) DFTB2- $\gamma^h$ +gaus, (D) DFTB3-diag, (E) DFTB3-diag+gaus, (F) DFTB3-Full+gaus, (G) DFTB3-3OB, and (H) CPMD simulations. The data depicted here is for one of the two independent trajectories. The reader should note the differences in scale of the horizontal axis between the various panels of the figure.

mechanism, almost to the extent of eliminating Grotthuss hopping and utilizing only vehicular transport. The favoring of the vehicular transport is due to the oversolvated hydroxide and the densely packed first solvation shell. In order for a successful hopping to occur, the hydrogen bonding topology of the proton donating water and proton accepting hydroxide must undergo large structural changes, which are unfavorable. It is also clear that PT is further hindered by the O–H repulsive potential in the third order method with the MIO parameter set, which effectively eliminates all Grotthuss PT mechanisms. Thus in DFTB3-diag+gaus and DFTB3-Full+gaus simulations, there are essentially only vehicular hydroxide transport.

The Grotthuss shuttling rate is calculated by the accumulation functions:

$$\begin{aligned} h(\Delta t) &= h(\Delta t - 1) + \Delta h(\Delta t) \\ h(0) &= 0 \end{aligned} \quad (7)$$

where  $\Delta t$  is the time step and  $\Delta h(\Delta t)$  is evaluated as follows:

$$\Delta h(\Delta t) = \begin{cases} 0, & \text{if no proton hop } (O_0 \text{ identity remains unchanged}) \\ 1, & \text{if the proton hops to a new donor} \\ -1, & \text{if the proton hops to the last donor} \end{cases} \quad (8)$$

In Figure 9, the Grotthuss shuttling rate for various DFTB methods is depicted. (The difference in the horizontal scale between the various figure panels should be noted.) The DFTB2 and DFTB2- $\gamma^h$  give similar result for proton hopping as the CPMD simulation. It is observed that there are long intervals of oscillatory shuttling. This makes the  $h(t)$  fluctuate around a value rather than increase successively as time passes. The O–H repulsive potential makes the hopping less frequent and extends the period of oscillatory shuttling. The third order method greatly hinders the hopping mechanism as expected, further suppressing hopping in the DFTB3-diag+gaus and

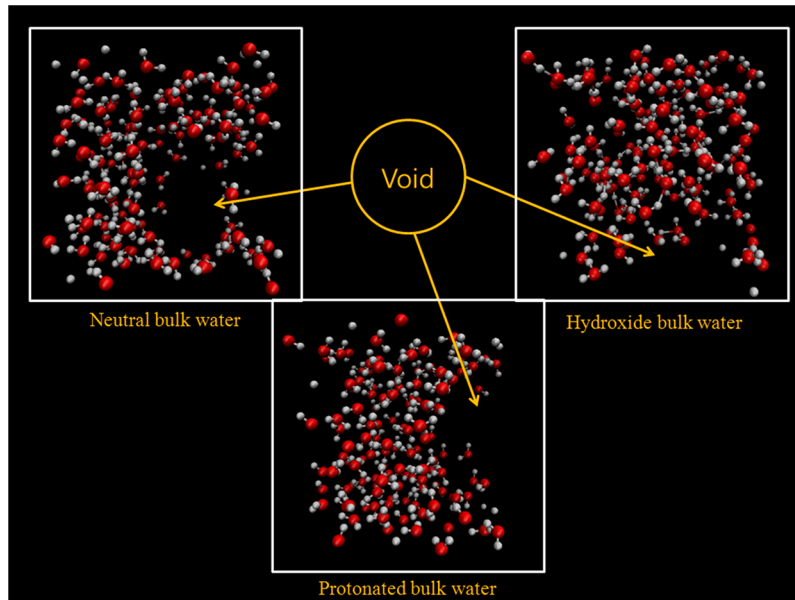


**Figure 10.** Snapshots of the neutral, hydroxide, and protonated bulk system after 50 ps of the MD time evolution using the DFTB3-diag+gaus method. The voids are detected in all simulations.

DFTB3-Full+gaus methods and resulting in essentially no successful Grotthuss hopping for the 50 ps trajectory. The DFTB3-3OB method improves the results over the MIO parameter set and predicts more frequent Grotthuss hopping events. This is in line with the lowered free energy barrier and may be attributed to the reduction in the coordination number of the  $\text{OH}^-$  ion, but the hopping frequency is still much lower than that determined from the CPMD method.

**3.4. DFTB Mechanism for Hydroxide Ion Transport.** A more detailed analysis on the DFTB hydroxide transport mechanism indicates that the DFTB methods captures some features of the dynamical coordination mechanism,<sup>4,5</sup> but fail to reproduce the entire picture. Here, the DFTB-3OB is taken as an example to illustrate the similarities and differences. Figure 12A shows the probability distribution for the number of HBs accepted by  $\text{O}_0$ , noted as  $P(n^*)$ .  $P(n^*)$  is largest at 5 and 6, with a small value at 4, which is in agreement with the hydroxide ion oversolvation issue we discussed in the section 3.3.1. The change in  $n^*$  near the PT event is analyzed in more detail in Figure 12B, by plotting  $n^*$  as a function of the PT reaction coordinate  $|\delta l|$ , denoted as  $n^*(|\delta l|)$ . It is observed that  $n^*(|\delta l|)$  is at its maximum value far from the PT event (large  $|\delta l|$  value), and decreases near the PT event (small  $|\delta l|$  value). This means the hydroxide ion becomes less solvated near the transition state, and this could be a driving force for the hydroxide transport in the DFTB mechanism. The PMFs for hydroxide ions with 4-, 5-, and 6-coordinated waters shown in Figure 12C further confirm the hypothesis that a decrease in coordination number drives the PT event. It is shown that the 4-coordinated hydroxide ions have a lower PT energy barrier than the 5-coordinated systems, which have a lower barrier compared to the 6-coordinated systems. For the 5- and 6-coordinated hydroxide ions, the energy barriers are larger than 2.5 kcal/mol and are unlikely to undergo PT events from thermal fluctuations. In fact, even if PT events do occur, they will not lead to a new stabilized  $\text{OH}^-[\text{H}_2\text{O}]_5$  or  $\text{OH}^-[\text{H}_2\text{O}]_6$  complex, and the proton will be most likely return to the original water oxygen in a short amount of time. In contrast, the

4-coordinated hydroxide ion has sufficiently low barrier for the PT.

However, one important feature of the DFTB mechanism that is qualitatively different from the dynamical hypercoordination mechanism is shown in the RDF of  $\text{H}'-\text{O}_w$ . Figure 12D. The  $\text{H}'-\text{O}_w$  RDF reveals that, for configurations both far and close to the PT event ( $|\delta l| > 0.5$  and  $|\delta l| < 0.1$ , respectively), the first peak is always pronounced. This indicates that the HB donated by the hydroxide ion is always present, and is qualitatively different from the dynamical hypercoordination mechanism, which predicts that the hydroxide ion only donates a HB close to the PT event (small  $|\delta l|$ ). It is interesting to see that this aspect of the DFTB mechanism is similar to that of the “traditional mirror image” mechanism, which also predicts a constantly donated HB by the hydroxide ion. However, “traditional mirror image” also differs from the DFTB mechanism in that it does not predict a reduction in the  $\text{O}_0$  coordination number near the PT event.<sup>4,5</sup> Therefore, the DFTB mechanism cannot be interpreted as either the “dynamical hypercoordination” or the “traditional mirror image” mechanism. It combines elements from these two qualitatively different mechanisms and forms a hydroxide transport mechanism of its own kind.

**3.5. Formation of Water Voids in the Simulation.** In all the SCC-DFTB methods, pockets of voids with no or very little water density were observed in the MD simulations. The formation of the voids was seen to occur in simulations of the hydrated excess proton, the hydrated hydroxide, and bulk water simulations with no ions. Figure 10 shows the snapshots of the bulk water, hydrated hydroxide, and hydrated excess proton system after 50 ps of NVT molecular dynamics simulations at a density of 0.97 g/mL using the DFTB3-diag+gaus method. It is noted that these voids also form in simulations in the constant NVE ensemble. The presences of significant voids were detected in all of the simulated systems, and these voids are found to fluctuate in size and position. This phenomenon is observed to occur primarily due to the overcoordinated water molecules. Due to the presence of the voids in the simulation

cell it is clear that not all portions of the system are completely solvated or solvated in a homogeneous fashion.

For all the SCC-DFTB methods, the water coordination number calculated from the  $O_w-O_w$  RDF (Figure 11) is larger

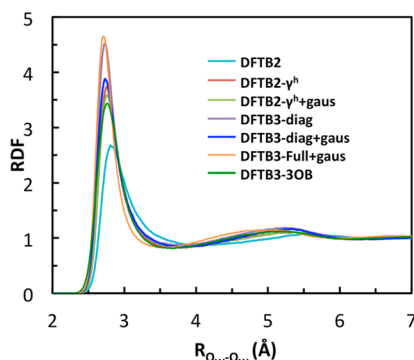


**Figure 11.** Radial distribution function for  $g_{O_w-O_w}(r)$  in hydrated hydroxide system. Data shown here includes DFTB2 (light blue), DFTB2- $\gamma^h$  (red), DFTB2- $\gamma^h$ +gaus (light green), DFTB3-diag (purple), DFTB3-diag+gaus (deep blue), DFTB3-Full+gaus (orange), and DFTB3-3OB (deep green) simulations.

by at least 1 compared to that calculated from the CPMD simulations using the HCTH120 functional,<sup>19</sup> which is in line with the results from Table 6 in ref 20 and results in ref 19. This indicates an increased water density in the first solvation shell that causes a density heterogeneity in the simulation box that was pre-equilibrated using the TIP3P water model at ambient pressure and temperature. Comparing DFTB2- $\gamma^h$  with DFTB2, it is observed that in the DFTB2- $\gamma^h$  method, the first and second peaks are more pronounced and their locations are shifted to the left (i.e., smaller separation distance). Also, the first peak is narrowed, indicating an increased localization. This observation is in agreement with ref 19 and implies that the

water molecules are closer to each other and become more ordered when the hydrogen-bonding correction is added. Combining the effect of the overcoordination of water molecules with the shortened first peak distance in the  $O_w-O_w$  RDF introduced by the  $\gamma^h$  function, the density is not likely to be physical and water void formation is almost unavoidable during constant volume simulation. It therefore seems likely that a SCC-DFTB simulation at constant NPT would reduce the simulation box volume and result in a water density significantly higher than reality.

#### 4. CONCLUSIONS

Presented here is a comparison of various SCC-DFTB methods and their predicted structural and dynamical properties for the hydrated hydroxide ion. The SCC-DFTB methods have been applied to small sized hydroxide water clusters,  $OH^--(H_2O)_n$ ,  $n = 4-7$ , and to simulations of the hydroxide ion in bulk water. Special attention has been given to newer SCC-DFTB versions, including the on-site and full third order term in the energy expansions based on the reference density, the modified O–H repulsive potential and the newest 3OB parameter set. These versions of the methodology are implemented because they have been shown to modestly improve the description of the hydrated excess proton in both gas-phase clusters and bulk water.<sup>20</sup> Interestingly, the results indicate that the original DFTB2 method and its hydrogen-bonding corrected variant more closely reproduce CPMD results while the incorporation of the O–H repulsive potential and the use of the third order correction with the original MIO parameter set effectively eliminate Grotthuss hopping and yield an oversolvated (hyper coordinated)  $OH^-$  ion that diffuses mainly through vehicular transport. The DFTB3-3OB parameter set outperforms the MIO parameter set for some of the structural, energetic and dynamic properties studied in this work, but it still does not outperform the accuracy of the DFTB2 methods. Importantly, the need for redesigning the parameters in the first and second

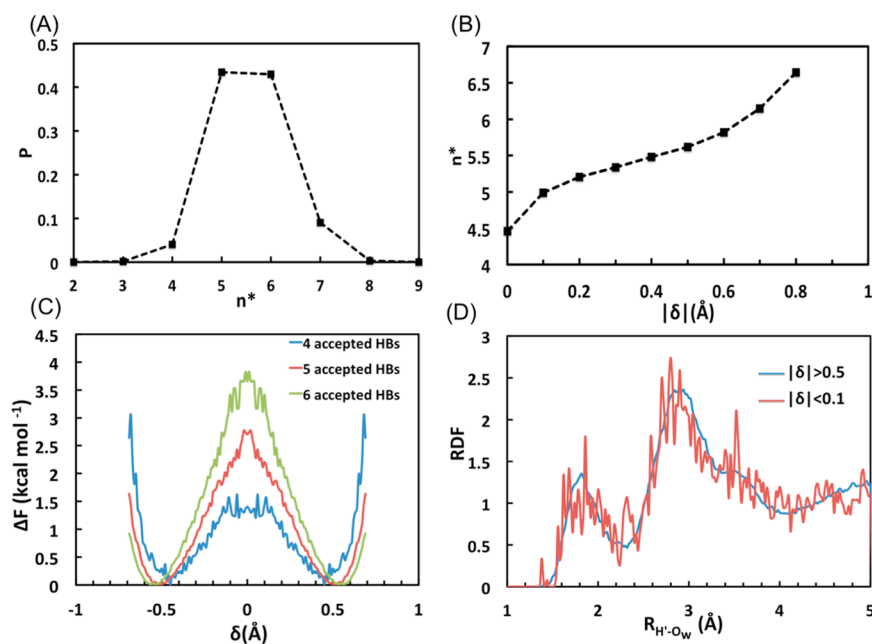


**Figure 12.** Results revealing hydroxide transport mechanism predicted by DFTB3-3OB method. (A) Probability distribution of number of hydrogen bonds accepted by  $O_0$ . (B) Number of hydrogen bonds accepted  $O_0$  as a function of  $|\delta|$ . (C) Proton transport reaction free energy profiles for different number of hydrogen bonds accepted by  $O_0$ . (D) Radial distribution function for  $g_{H^-O_w}(r)$  at both large and small  $|\delta|$ .

terms of eq 1 to improve the accuracy of DFTB3 may imply that the physically motivated third order term alone does not necessarily improve the accuracy of the SCC-DFTB method, and for system such as hydroxide ions solvated in bulk water it may even produce worse result than the DFTB2 method. Therefore, it is possible that the accuracy of the SCC-DFTB method is more limited by the approximations and empiricism in the first and second term of eq 1 than by the early truncation at the second order expansion.<sup>44–46</sup> In addition, the over-coordination issue of the underlying SCC-DFTB water model causes increased local water density and water voids in constant volume simulations of the hydrated excess proton, the hydrated hydroxide, and bulk water. The present results highlight the extreme difficulties in formulating an accurate, yet efficient, approximate QM approach for the simulation of aqueous and related condensed phase systems. However, our results can serve as important benchmarks for future improvement of the SCC-DFTB methodology.

## APPENDIX

Shown in Figure 13 are the distributions of potential energy minima of  $\text{OH}^-(\text{H}_2\text{O})_n$ ,  $n = 4–7$ , found using the basin hopping Monte Carlo procedure with the DFTB2- $\gamma^h$  method.

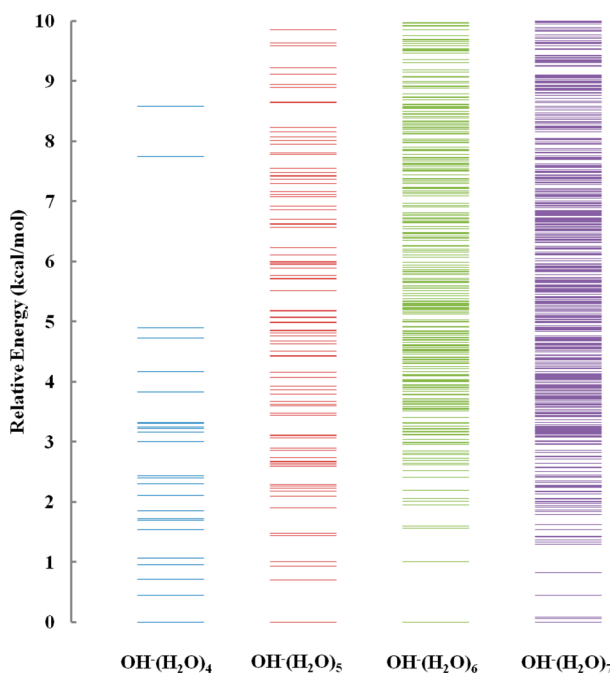


**Figure 13.** Distributions of potential energy minima of the  $\text{OH}^-(\text{H}_2\text{O})_n$  clusters, for  $n = 4–7$ , calculated from the basin hopping Monte Carlo procedure with the DFTB2- $\gamma^h$  method.

## AUTHOR INFORMATION

### Corresponding Author

\*E-mail: gavoth@uchicago.edu. Fax: 773-795-9106. Phone: 773-702-9092.

### Author Contributions

†T.H.C. and R.L. contributed equally to this work.

### Notes

The authors declare no competing financial interest.

## ACKNOWLEDGMENTS

This research was supported by the National Science Foundation (NSF grant CHE-1214087). The authors would like to acknowledge the support from KISTI supercomputing center through the strategic support program for the supercomputing application research [No. KSC-2011-C2-31].

## REFERENCES

- (1) Knight, C.; Voth, G. A. *Acc. Chem. Res.* **2012**, *45*, 101.
- (2) Swanson, J. M. J.; Maupin, C. M.; Chen, H.; Petersen, M. K.; Xu, J.; Wu, Y.; Voth, G. A. *J. Phys. Chem. B* **2007**, *111*, 4300.
- (3) Ludwig, R. *Angew. Chem., Int. Ed.* **2003**, *42*, 258.
- (4) Tuckerman, M. E.; Chandra, A.; Marx, D. *Acc. Chem. Res.* **2006**, *39*, 151.
- (5) Marx, D.; Chandra, A.; Tuckerman, M. E. *Chem. Rev.* **2010**, *110*, 2174.
- (6) Marx, D. *ChemPhysChem* **2006**, *7*, 1848.
- (7) Xie, W.; Gao, J. *J. Chem. Theory Comput.* **2007**, *3*, 1890.
- (8) Song, L.; Han, J.; Lin, Y.; Xie, W.; Gao, J. *J. Phys. Chem. A* **2009**, *113*, 11656.
- (9) Elstner, M.; Porezag, D.; Jungnickel, G.; Elsner, J.; Haugk, M.; Frauenheim, T.; Suhai, S.; Seifert, G. *Phys. Rev. B* **1998**, *58*, 7260.
- (10) Elstner, M.; Hobza, P.; Frauenheim, T.; Suhai, S.; Kaxiras, E. *J. Chem. Phys.* **2001**, *114*, 5149.
- (11) Cui, Q.; Elstner, M.; Kaxiras, E.; Frauenheim, T.; Karplus, M. *J. Phys. Chem. B* **2001**, *105*, 569.
- (12) Elstner, M.; Cui, Q.; Munih, P.; Kaxiras, E.; Frauenheim, T.; Karplus, M. *J. Comput. Chem.* **2002**, *24*, 565.
- (13) Lin, C. S.; Zhang, R. Q.; Lee, S. T.; Elstner, M.; Frauenheim, T.; Wan, L. *J. J. Phys. Chem. B* **2005**, *109*, 14183.
- (14) Kruger, T.; Elstner, M.; Schiffels, P.; Frauenheim, T. *J. Chem. Phys.* **2005**, *122*, 114110.
- (15) Zhechkov, L.; Heine, T.; Patchkovskii, S.; Seifert, G.; Duarte, H. A. *J. Chem. Theory Comput.* **2005**, *1*, 841.
- (16) Riccardi, D.; Schaefer, P.; Yang, Y.; Yu, H.; Ghosh, N.; Prat-Resina, X.; König, P.; Li, G.; Xu, D.; Guo, H.; Elstner, M.; Cui, Q. *J. Phys. Chem. B* **2006**, *110*, 6458.
- (17) Elstner, M. *Theor. Chem. Acc.* **2006**, *116*, 316.
- (18) Choi, T. H.; Jordan, K. D. *J. Phys. Chem. B* **2010**, *114*, 6932.
- (19) Maupin, C. M.; Aradi, B.; Voth, G. A. *J. Phys. Chem. B* **2010**, *114*, 6922.
- (20) Goyal, P.; Elstner, M.; Cui, Q. *J. Phys. Chem. B* **2011**, *115*, 6790.
- (21) Gaus, M.; Cui, Q.; Elstner, M. *J. Chem. Theory Comput.* **2011**, *7*, 931.
- (22) Choi, T.-H. *Chem. Phys. Lett.* **2012**, *543*, 45.
- (23) Ohta, Y.; Okamoto, Y.; Irle, S.; Morokuma, K. *ACS Nano* **2008**, *2*, 1437.
- (24) Qian, H. J.; Duin, A. C. T.; Morokuma, K.; Irle, S. *J. Chem. Theory Comput.* **2011**, *7*, 2040.
- (25) Yang, Y.; Yu, H.; Elster, M.; Cui, Q. *J. Chem. Theory Comput.* **2008**, *4*, 2067.
- (26) Xu, D.; Guo, H.; Cui, Q. *J. Phys. Chem. A* **2007**, *111*, 5630.
- (27) Dewar, M. J. S.; Zoebisch, E.; Healy, E. F.; Stewart, J. J. P. *J. Am. Chem. Soc.* **1985**, *107*, 3902.
- (28) Stewart, J. J. P. *J. Comput. Chem.* **1989**, *10*, 209.
- (29) Ventura, O. N.; Coitino, E. L.; Lledo, A.; Bertean, J. *J. Mol. Struct.: THEOCHEM* **1989**, *187*, 55.
- (30) Csonka, G. I. *J. Comput. Chem.* **1993**, *14*, 895.
- (31) Csonka, G. I.; Angyan, J. G. *J. Mol. Struct.: THEOCHEM* **1997**, *393*, 31.
- (32) Sattelmeyer, K. W.; Tirado-Rives, J.; Jorgensen, W. L. *J. Phys. Chem. A* **2006**, *110*, 13551.
- (33) Islam, S. M.; Roy, P. N. *J. Chem. Theory Comput.* **2012**, *8*, 2412.
- (34) Gaus, M.; Goez, A.; Elstner, M. *J. Chem. Theory Comput.* **2013**, *9*, 338–354.
- (35) Riccardi, D.; König, P.; Prat-Resina, X.; Yu, H. B.; Elstner, M.; Frauenheim, T.; Cui, Q. *J. Am. Chem. Soc.* **2006**, *128*, 16302.
- (36) Wales, D. J.; Scheraga, H. A. *Science* **1999**, *285*, 1368.

- (37) Doye, J. P.; Wales, D. J. *J. Chem. Soc., Faraday Trans.* **1997**, *93*, 4233.
- (38) Doye, J. P.; Wales, D. J. *Phys. Rev. B* **1999**, *59*, 2292.
- (39) Doye, J. P.; Wales, D. J.; Miller, M. A. *J. Chem. Phys.* **1998**, *109*, 8143.
- (40) Aradi, B.; Hourahine, B.; Frauenheim, T. *J. Phys. Chem. A* **2007**, *111*, S678.
- (41) Monkhorst, H. J.; Pack, J. D. *Phys. Rev. B* **1976**, *13*, 5188.
- (42) Roberts, S. T.; Petersen, P. B.; Ramasesha, K.; Tokmakoff, A.; Ufimtsev, I. S.; Martinez, T. J. *Proc. Natl. Acad. Sci. U.S.A.* **2009**, *106*, 15154.
- (43) Ufimtsev, I. S.; Kalinichev, A. G.; Martinez, T. J.; Kirkpatrick, R. *J. Phys. Chem. Chem. Phys.* **2009**, *11*, 9420–9430.
- (44) Giese, T. J.; York, D. M. *J. Chem. Phys.* **2010**, *133*, 244107.
- (45) Giese, T. J.; York, D. M. *J. Chem. Phys.* **2011**, *134*, 194103.
- (46) Giese, T. J.; York, D. M. *Theor. Chem. Acc.* **2012**, *131*, 1145.